Environ Geochem Health
DOI 10.1007/s10653-017-9947-0

ORIGINAL PAPER

Date palm waste-derived biochar composites with silica and zeolite: synthesis, characterization and implication for carbon stability and recalcitrant potential

Munir Ahmad · Mahtab Ahmad · Adel R. A. Usman · Abdullah S. Al-Faraj · Adel Abduljabbar · Yong Sik Ok · Mohammad I. Al-Wabel

Received: 31 December 2016 / Accepted: 17 March 2017

Abstract Engineered organo-mineral composites were synthesized from date palm waste biochar and silica or zeolite via mechanochemical treatments. Date palm tree rachis (leaves) waste biomass was pre-treated with silica or zeolite minerals via ball milling and sonication prior to pyrolysis at 600 °C. The resultant organo-mineral composites and pristine materials were characterized using X-ray diffraction, thermogravimetric–differential thermal (TG–DTA), Fourier transform infrared, scanning electron microscope analyses and surface area and porosity analyzer to investigate the variations in physiochemical and structural characteristics. Compared to the resultant composites derived from non-milled date palm biomass, ball milling increased surface area, while decreased crystallinity index and effective particle size of the biochar composites. Silica composited biochars were located near origin in the van Krevelen diagram indicating lowest H/C and O/C molar ratios, thus suggesting higher aromaticity and lower polarity compared to other biochars. TGA thermograms indicated highest thermal stability of silica composited biochars. Ash and moisture corrected TGA thermograms were used to calculate recalcitrance index (R_{50}) of the materials, which speculated high degradability of biomass ($R_{50} < 0.4$), minimal degradability of biochars and zeolite composited biochars ($0.5 < R_{50} < 0.7$) and high recalcitrant nature of silica composited biochars ($R_{50} > 0.7$). Silica composited biochars exhibited highest carbon sequestration potential (64.17–95.59%) compared to other biochars.

Electronic supplementary material The online version of this article (doi:10.1007/s10653-017-9947-0) contains supplementary material, which is available to authorized users.

M. Ahmad · M. Ahmad · A. R. A. Usman · A. S. Al-Faraj · M. I. Al-Wabel (✉)
Soil Sciences Department, College of Food and Agricultural Sciences, King Saud University, P.O. Box 2460, Riyadh 11451, Kingdom of Saudi Arabia
e-mail: malwabel@ksu.edu.sa

M. Ahmad
Department of Environmental Sciences, Faculty of Biological Sciences, Quaid-I-Azam University, Islamabad 45320, Pakistan

A. R. A. Usman
Department of Soils and Water, Faculty of Agriculture, Assiut University, Assiut 71526, Egypt

A. Abduljabbar
Industrial Psychology, College of Education, King Saud University, Riyadh, Saudi Arabia

Y. S. Ok
Korea Biochar Research Center and Department of Biological Environment, Kangwon National University, Chuncheon 200-701, Republic of Korea

Published online: 23 March 2017

Highest recalcitrance and carbon sequestration potential of silica composited biochars may be attributed to changes in structural arrangements in the silica–biochar complex. Encapsulations of biochar particles with amorphous silica via Si–C bonding may have prevented thermal degradation, subsequently increasing recalcitrance potential of silica composited biochars.

Keywords Carbon sequestration · Engineered biochar · Organo-mineral · Recalcitrance index · Encapsulation

Introduction

The shift from natural to agricultural ecosystem has lost about 20–80 tons ha^{-1} of carbon (C), resulting in reduced soil and water quality, and biomass productivity (Lal 2004). To augment soil fertility and productivity, C from atmospheric carbon dioxide (CO_2) must be transferred to soil C pool. Biochar production and usage in soil is the possible option to reduce atmospheric CO_2 and increase soil C pool (Fowles 2007; Laird 2008). Climate change mitigation potential of biochar is due to its high recalcitrance nature, which slows down the rate of transferring photosynthetically fixed C in biomass to the atmosphere (Schmidt and Noack 2000; Kuzyakov et al. 2009). Conversion of biomass to biochar yields more stable C as it sequesters about 50% of the initial C, which can be retained in the soil for 100–1000 years, compared with burning or direct dumping of biomass in the soil which retains C in the soil for only 5–10 years (Lehmann et al. 2006). Besides enhancing soil C pool, other advantages associated with biochar include enhancing soil fertility and productivity, reducing nutrient losses, increasing water-holding capacity of the soil, immobilizing the heavy metals and cost-effectiveness (Lehmann and Joseph 2009; Lenton and Vaughan 2009; Ahmad et al. 2014a). However, C sequestration and recalcitrance potential of biochar depend on physiochemical characteristics, type and composition of the biomass, and pyrolysis temperature. Due to the presence of a range of partially to completely carbonized C forms, crystalized C forms, non-polyaromatic C and ash contents in various biomass types, biochar is characterized as heterogeneous material (Keiluweit et al. 2010; Zimmermann et al. 2012). Therefore, prediction of C sequestration or recalcitrance potential of biochar is ambiguous. Aromatic carbons are critical in determining the recalcitrance potential of the biochar because CO_2 production initiates from polycyclic aromatic components of biochar (Zimmermann et al. 2012).

It is well elaborated now that all biochars are not equal in their properties and performance. There is a recent surge of interest to obtain biochar with specific characteristics for a specific purpose. In this context, research is in progress to optimize feedstock type, pyrolysis conditions and pre- or post-modification of the biochar to have the desired product. Modification of biochar for improved surface and structural properties for efficient environmental benefits has been started recently (Ok et al. 2015). These modifications can be physical, chemical, impregnation with mineral sorbents, mechanical treatments and magnetic modifications (Rajapaksha et al. 2016). Engineered or designer biochar can be synthesized through treatment of biomass with the foreign material prior to pyrolysis, treatment of biochar with foreign materials, mechanical treatment of biomass or biochar and compositing the biochar with foreign materials. These modifications may improve surface characteristics, functional groups, pore volume and sorption capacities of the biochar (Rajapaksha et al. 2016). Recently, mineral components such as montmorillonite, bentonite and kaolinite have been used to make clay-supported biochar composites (Fosso-kankeu et al. 2015; Yao et al. 2014). Due to higher surface charge, higher ion exchange capacity, lamellar structure and negative surface change, clay minerals such as zeolite have widely been used in the soil for contaminants removal (Bilgic 2005; Gurses et al. 2006). Zeolite exhibits a strong electric field which interacts with quadrupole moment of CO_2 and captures it (Bonenfant et al. 2008). Nano-sized silica, due to higher specific surface area and hydrothermal stability is being used to modify surface chemistries of various materials. Therefore, the minerals such as silica and zeolite if composited with biochar may change the physiochemical and structural composition of biochar through fusion and sintering during pyrolysis resulting in changes in C aromatic structures (Xiao et al. 2014; Rumpel et al. 2007). As silica and zeolite are non-toxic and chemically more stable, their composites with biochar may have greater potential to be applied as

sorbents and soil amendments (Wang et al. 2016). These minerals may arrange the heterogeneous structure and reduce C evolution by encapsulating it in the structure, thereby resulting in higher recalcitrance when applied in soil (Guo and Chen 2014).

Hence, it could be hypothesized that organo-mineral biochar produced by mixing silica and zeolite minerals with biomass feedstock prior to pyrolysis may result in a newly developed composites having improved characteristics for recalcitrance potential and higher C stability. Therefore, the objectives of this study are to: (1) synthesis organo-mineral composites by pyrolysis of biomass feedstock after mixing with silica and zeolite minerals; and (2) characterize the produced organo-mineral composites in terms of recalcitrance potential and C stability.

Materials and methods

Materials preparation

Date palm tree waste rachis were collected from the agricultural farms in Riyadh, Saudi Arabia, dried and cut into small pieces (2.5–5 cm). The waste was grinded using a mechanical grinder, sieved through 0.6-mm screen, stored in airtight bags and named as BM. White sand (silica) was sieved through 0.6-mm screen, washed with deionized water (DI), 10% HCl, 30% H_2O_2 solutions and finally with DI water several times to remove carbonates, organic matter and other impurities. Washed silica sand (S) was dried in air and stored in airtight jars. Zeolite (Clinoptilolite 25523) was purchased from San Bernardino Co. PO Box. 591 Clarkson, New York. Zeolite (Z) was grinded and sieved through 0.6-mm screen. Prepared silica sand, zeolite and date palm tree waste biomass were milled in a ball mill (Fritsch Pulverisette 7, Germany) at 800 rpm for 20 min.

Biochar composites synthesis

To impregnate biomass with silica or zeolite, a method described by Yao et al. (2014) was followed with little modifications (mineral–biomass suspension was stirred for 3 h instead of 1 h). Specifically, 4 g of powdered silica or zeolite was added in 1000 mL DI water and sonicated with Sonics Vibra-Cell VCX-500 Ultrasonic Processor for 30 min at 35 AMP. 20 g of each ball-milled or non-milled date palm tree waste biomass (MBM and BM, respectively) was added into the suspension and stirred on a magnetic stirrer for 3 h. Silica and zeolite impregnated biomass were separated from the mixture and dried at 80 °C.

Date palm tree waste biomass (BM), milled biomass (MBM), silica impregnated biomass (BM + S), silica impregnated milled biomass (MBM + S), zeolite impregnated biomass (BM + Z) and zeolite impregnated milled biomass (MBM + Z) were kept in loosely covered crucibles and slowly pyrolyzed (5 °C per min) in a tube furnace (Carbolite TZF 12/100/900, UK) in oxygen-limited environment at 600 °C for 3 h. The resulting biochar (BC), milled biochar (MBC), silica composited biochar (BC + S), silica composited milled biochar (MBC + S), zeolite composited biochar (BC + Z) and zeolite composited milled biochar (MBC + Z) were kept in a desiccator for 30 min. After weighing, resultants composites were washed thrice with DI water, dried in an oven and stored in air tight containers.

Biochar characterization

Date palm tree waste biomass and derived biochar composites were subjected to proximate, ultimate and chemical characterization.

Yield, proximate and chemical analyses

The percent yield of the produced biochar composites was calculated as:

$$Yield\,(\%) = \frac{Weight\ of\ Biomass - Weight\ of\ Biochar}{Weight\ of\ Biomass} \times 100 \quad (1)$$

Proximate analysis, including moisture, ash contents and volatile matter of the materials were obtained following the standard method of ASTM D1762-84 (ASTM 1989), while the resident matter was calculated with difference method. Electrical conductivity (EC) and pH of the materials were determined in 1:10 suspension in DI water. Cation exchange capacity (CEC) of the materials was measured by the ammonium acetate extraction method (Hendershot et al. 2008). Active carbon fraction was determined following the method described by Blair et al. (1995). Non-labile carbon fraction was calculated by the difference between active carbon and total carbon.

Ultimate analysis

Elemental composition of biomass and biochar composites was assessed through CHNSO elemental analyzer (series II, PerkinElmer, USA). Percent C, H, N and S were measured by the instrument, while O was calculated using the following equation:

$$\mathrm{O}\ (\%) = 100 - (\mathrm{C} + \mathrm{H} + \mathrm{N} + \mathrm{S} + \text{ash}\ \%) \quad (2)$$

Atomic ratios of the elements such as O/C and H/C were also calculated to present the polarity and aromaticity of the materials, respectively.

SEM, TGA, FTIR, XRD and BET analyses

To observe surface morphology and structural changes induced by milling and impregnation with minerals (silica and zeolite), composite materials (before and after pyrolysis) were analyzed using scanning electron microscope (SEM; EFI S50 Inspect, the Netherlands). Samples were spread on aluminum stubs coated with adhesive carbon tapes (12 mm; PELCO, UK) and coated with nano-gold particles for 60 s using 108 Auto/SE Sputter Coater (Ted Pella Inc. USA). Images were taken in the range of 2000–300× magnification at an acceleration voltage of 30 kV under high vacuum. Thermal stability of pre- and post-pyrolyzed composites was analyzed using thermogravimetric analyzer (DTG-60H, Shimadzu, Japan). Weight loss of the materials was recorded with the rise in temperature from 0 to 1100 °C. The composition of structural and functional groups of pre- and post-pyrolyzed composite materials was determined using Fourier transforms infrared spectroscopy (FTIR, Bruker Alpha-Eco ATR-FTIR, Bruker Optics Inc). To analyze various mineralogical phases of the materials, X-ray diffractometer (MAXima_X XRD-7000, Shimadzu, Japan) was used with 30 mA Cu Kα radiation at the scan speed of 2 degree min^{-1} in continuous scan mode. Surface area, total pore volume and pore diameter were analyzed through Brunauer–Emmett–Teller (BET) method using surface area and porosity analyzer (TriStar II 3020, Micromeritics, USA).

Thermal stability calculation

Relative thermal degradability of the materials was quantified using TGA analysis data by calculating recalcitrance index (R_{50}) proposed by Harvey et al. (2012) using following equation:

$$R_{50} = T_{50,x}/T_{50,\text{graphite}} \quad (3)$$

where $T_{50,x}$ and $T_{50,\text{graphite}}$ are the temperatures of moisture and ash corrected TG thermograms (weight loss due to C oxidation only) at 50% weight loss by volatilization or oxidation of the materials and graphite, respectively. To correct the TG thermograms for moisture and ash contents, the following expression was applied (Harvey et al. 2012):

$$W_{i,\text{cor}} = 100 + \left[100 \times \left(W_{i,\text{uncor}} - W_{200,\text{uncor}}\right)/\left(W_{200,\text{uncor}} - W_{\text{cutoff,uncor}}\right)\right] \quad (4)$$

where $W_{i,\text{cor}}$ and $W_{i,\text{uncor}}$ are corrected and uncorrected percent weight loss of the initial sample, respectively, while $W_{200,\text{uncor}}$ is the percent weight loss of the initial sample up to 200 °C (corresponding to water loss in the sample). $W_{\text{cutoff,uncor}}$ represents weight loss at the temperature where no more oxidation takes place.

Percent carbon sequestration potential (*CS*) was calculated using the equation given by Zhao et al. (2013).

$$\mathrm{CS}\ (\%) = \frac{Yield\ (\%) \times C\%\ Biochar \times R_{50}}{C\%\ Feedstock} \quad (5)$$

where C is percent carbon contents.

Crystallinity and effective particle size calculation

XRD intensities were used to calculate crystallinity index (CrI) to investigate the influence of ball milling on the crystallinity of cellulose using following equation (Murillo et al. 2014).

$$\mathrm{CrI}\ (\%) = \frac{I_{002} - I_{18}}{I_{002}} \times 100 \quad (6)$$

where I_{002} is the maximum intensity of the crystalline cellulose at $2\theta = 22.8°$, while I_{18} is the crystallinity of cellulose at $2\theta = 18°$.

The average effective particle size (EPS) of each composite material was calculated by modifying the equation given by Lowell et al. (2004).

$$\textit{Effective particle size}\ (\mathrm{EPS}) = \left[\frac{3}{\rho \times S}\right] \times 2 \quad (7)$$

where S represent surface area analyzed by BET and ρ is the density of each material analyzed using core method. Dried material was filled in a cylinder of known volume and weight. The weight of the material was calculated by subtracting cylinder weight from total, and volume of the material was taken equivalent to the volume of a cylinder. The density of the material was obtained by dividing weight by the volume.

Results and discussion

Yield, proximate and chemical analyses

Yield, proximate composition and chemical analyses of date palm tree waste biochar and derived composites are presented in Table 1. Based on the mass loss during pyrolysis, silica composited biochar (BC + S) exhibited highest yield (55.12%) among all the materials, while lowest (31.78%) was found in milled biochar (MBC). Yield followed the order of silica composited biochar > zeolite composited biochar > biochar. Silica and zeolite composited biomass contained the same amount of minerals (silica or zeolite); therefore, the higher yield of silica composited biochar suggested more thermal stability of silica than zeolite. Highest yield of silica and zeolite composited biochars could be due to highly resistant nature of silica and zeolite against thermal degradation. With thermalization, volatile matter reduced, while resident matter and ash contents were concentrated. The highest increase in the resident matter was observed in MBC (59%), followed by BC (52%), and lowest was recorded in BC + S (40%) compared to their biomass. The highest increase in ash contents was observed in BC and MBC (78%), and lowest in BC + Z (58%). pH of the biomass ranged from 5.94 to 6.32, which increased with pyrolysis between the range of 8.85–10.23, indicating the alkaline nature of the biochars. Increase in pH was due to increase in basic functional groups, alkali salt separation from organic compounds and reduction in acidic functional groups (Mukherjee et al. 2011). This might be due to the reason that when pyrolysis undergoes, most of the volatiles vent out while recalcitrant cationic species and exchangeable cations (Ca^{2+}, Mg^{2+} and Na^{+}) condensate in the biochar resulting in higher pH (Inyang et al. 2010). The concentration of recalcitrant cationic species, therefore, may help biochar to be stable for longer time. With pyrolysis, CEC of the produced biochars

Table 1 Proximate and chemical analyses results of date palm tree leaves waste biomass and its derived biochars

	Yield (%)	Moisture (%)	Volatile matter (%)	Resident matter (%)	Ash (%)	pH (1:10)	Cation exchangeable capacity (cmol kg^{-1})
BM	–	4.98 ± 0.04	62.22 ± 2.32	24.47 ± 2.36	8.33 ± 0.01	5.94 ± 0.00	70.30 ± 1.07
MBM	–	4.77 ± 0.03	66.36 ± 5.53	20.50 ± 5.72	8.36 ± 0.21	5.95 ± 0.00	66.01 ± 0.00
BM + S	–	9.06 ± 1.39	51.86 ± 1.56	13.40 ± 6.64	25.68 ± 6.47	6.04 ± 0.08	63.32 ± 1.15
MBM + S	–	3.36 ± 0.50	58.33 ± 6.70	9.89 ± 9.21	28.41 ± 3.02	6.13 ± 0.01	70.36 ± 1.08
BM + Z	–	0.82 ± 0.31	56.68 ± 7.42	13.59 ± 8.38	28.91 ± 1.28	6.28 ± 0.13	108.78 ± 2.24
MBM + Z	–	1.30 ± 0.21	62.77 ± 6.30	9.44 ± 8.18	26.50 ± 2.09	6.32 ± 0.01	104.48 ± 1.26
BC	41.32 ± 0.61	1.01 ± 0.09	8.93 ± 1.13	51.39 ± 0.70	38.68 ± 0.34	10.23 ± 0.01	39.86 ± 0.71
MBC	31.78 ± 4.78	1.58 ± 0.75	10.05 ± 1.49	50.10 ± 0.98	38.27 ± 1.26	10.10 ± 0.02	57.83 ± 13.26
BC + S	55.12 ± 1.38	0.53 ± 0.52	5.76 ± 1.01	22.32 ± 7.83	71.39 ± 9.37	9.02 ± 0.01	33.20 ± 0.93
MBC + S	43.54 ± 2.27	0.73 ± 0.10	7.59 ± 0.21	16.12 ± 0.32	75.57 ± 0.02	8.85 ± 0.04	41.27 ± 0.84
BC + Z	51.73 ± 0.88	0.00 ± 0.00	9.49 ± 0.03	22.14 ± 02.0	68.37 ± 0.23	9.09 ± 0.02	76.27 ± 0.47
MBC + Z	41.83 ± 4.27	0.00 ± 0.00	10.87 ± 1.28	8.86 ± 1.37	80.27 ± 0.09	9.37 ± 0.01	86.43 ± 0.65

BM biomass, *MBM* milled biomass, *BM + S* biomass composite with silica, *MBM + S*, milled biomass composite with silica, *BM + Z* biomass composite with zeolite, *MBM + Z* milled biomass composite with zeolite, *BC* biochar, *MBC* milled biochar, *BC + S* biochar composite with silica, *MBC + S* milled biochar composite with silica, *BC + Z* biochar composite with zeolite, *MBC + Z* milled biochar composite with zeolite

decreased significantly compared to the feedstocks. The maximum reduction in CEC was observed in BC + S (47.57%), while the minimum was in MBC (12.39%). Reduced CEC in biochars might be due to the loss of surface functional groups and increased carbon aromaticity (Joseph et al. 2010).

X-ray diffraction analysis

XRD spectra of date palm tree waste biomass, its derived biochar composites, silica and zeolite are presented in Fig. 1. Different visible peaks on the spectra confirm the existence of inorganic materials and crystalline minerals in the materials. Peaks of clinoptilolite (zeolite) in XRD pattern of raw zeolite were identified at $2\theta = 9.82$, 11.14, 13.04, 19.06 and 22.29. Similarly, clinoptilolite peaks were also shown in zeolite composited biomass and biochars with little shifts in peaks. Peaks at $2\theta = 20.88$ and 26.68 were designated as SiO_2, while a peak at $2\theta = 50.18$ was designated as feldspar in raw silica sample. SiO_2 and feldspar were also identified in silica composited biomass and biochars with shifts in peak location compared to silica sample. Two peaks of a carbon-containing mineral mellite ($Al_2[C_6(COO)_6].16H_2O$) appeared at $2\theta = 11.6$ and 21.48 in all the biomass samples (Usman et al. 2015). In biochar samples, mellite was lost during pyrolysis of the biomass (Fig. 1a), while it was still present with reduced peak intensity in silica and zeolite composited biochars (Fig. 1b, c). Reduction in peak intensity of the sylvite (KCl) and calcite ($CaCO_3$) was more in BC (Fig. 1a) compared to silica and zeolite composited biochars. Shifting in peak location is an indication of interactions between mineral and biomass or biochar during composite synthesis. Shifts in peak positions as associated with pyrolysis are presented in Table S1 (supplementary material). A peak of clinoptilolite at $2\theta = 13.04$ in zeolite sample was shifted to 13.30 and 13.38 in BM + Z and MBM + Z, respectively, and to 13.42 and 13.48 in BC + Z and MBC + Z, respectively. Likewise, a peak of clinoptilolite at $2\theta = 16.88$ in zeolite sample was shifted to 17.24 and 17.26 in BM + Z and MBM + Z, respectively, and to 26.54 in BC + Z and MBC + Z. A peak designated as SiO_2 was shifted to 26.58 and 26.24 in BM + S and MBM + S, respectively, and to 26.62 and 26.60 in BC + S and MBC + S, respectively, from 26.68 in silica sample. These shifts in peaks of XRD patterns suggested the formation of complexations between minerals (silica and zeolite) and biochars during composites synthesis.

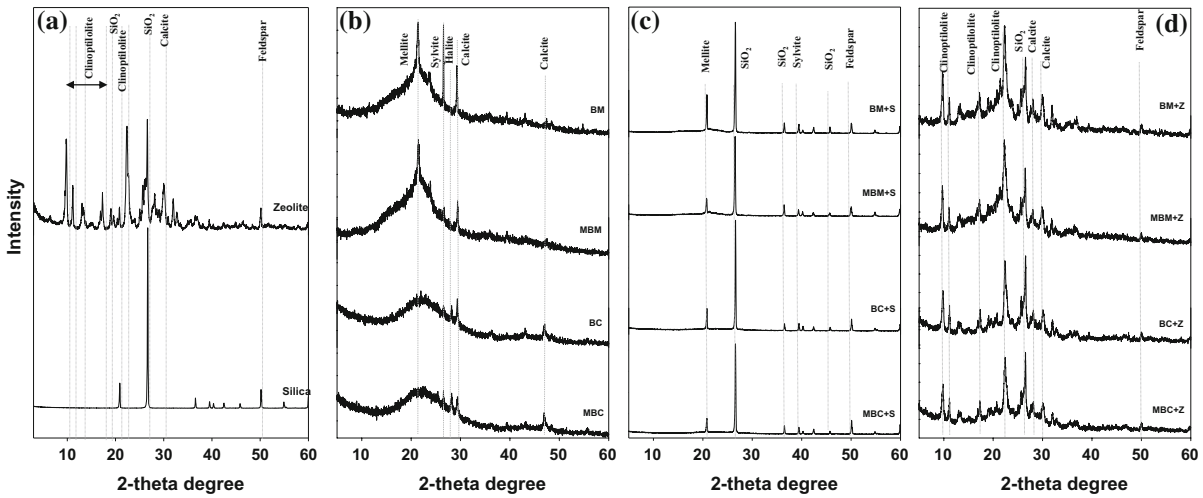

Fig. 1 XRD patterns of (**a**) pristine zeolite and silica powders, **b** date palm tree rachis waste biomass and its derived biochars, **c** silica composited biomass and its derived biochar, (**d**) zeolite composited biomass and its derived biochars. (BM, biomass; MBM, milled biomass; BM + S, biomass composite with silica; MBM + S, milled biomass composite with silica; BM + Z, biomass composite with zeolite; MBM + Z, milled biomass composite with zeolite; BC, biochar; MBC, milled biochar; BC + S, biochar composite with silica; MBC + S, milled biochar composite with silica; BC + Z, biochar composite with zeolite; MBC + Z, milled biochar composite with zeolite)

BET surface area

Surface area, pore size and pore volume of the date palm tree waste-derived biomass and biochars are shown in Table 2. It is obvious from the results that pyrolysis has increased the BET surface area up to 99.8% in biochar compared to the biomass. The maximum surface area was observed for MBC (198.359 $m^2\ g^{-1}$), followed by BC (164.731 $m^2\ g^{-1}$), while MBC + S showed the lowest BET surface area (124.73 $m^2\ g^{-1}$) among different biochars. Compared to silica composited biochar, zeolite composited biochar exhibited higher surface area, which was due to higher surface area of zeolite (19.854 $m^2\ g^{-1}$) than that of silica (0.640 $m^2\ g^{-1}$). Low BET surface area in silica and zeolite composite biochars compared to BC and MBC could be due to plugging of pores in the presence of minerals and high ash contents (Table 1). Yao et al. (2014) also reported that reduced surface area of clay-enriched biochar composites could be due to blockage of biochar pores with clay mineral particles. Pore size was reduced to ~5–10 nm in biochars compared to ~25–39 nm in biomass due to evaporation of volatile material and condensation of aromatic structure. Minerals in biochar composites may have blocked the small sized pores, thus giving rise to slightly higher pore size in silica and zeolite composited biochars. Total pore volume in mineral (silica and zeolite) composites biochars was lower as compared to biochar. Reduction in pore volume in silica and zeolite composited biochars could be due to blockage of the mesopores (2–50 nm) with the mineral particles (Rawal et al. 2016).

Table 2 Surface area, pore size and pore volume analyses results of date palm tree leaves waste biomass and its derived biochars

	Surface area ($m^2\ g^{-1}$)	Pore size (nm)	Total volume in pores ($cm^3\ g^{-1}$)
BM	0.463	24.565	0.00019
MBM	0.393	28.420	0.00021
BM + S	0.377	33.578	0.00021
MBM + S	0.415	39.023	0.00019
BM + Z	0.838	29.029	0.00047
MBM + Z	1.783	33.135	0.00031
BC	164.731	4.919	0.09746
MBC	198.359	5.614	0.10690
BC + S	140.374	6.052	0.06800
MBC + S	124.730	6.023	0.05400
BC + Z	153.278	8.708	0.07114
MBC + Z	134.766	9.843	0.06075
Zeolite	19.8541	30.1159	0.00563
Silica	0.6405	29.6291	0.00030

BM biomass, *MBM* milled biomass, *BM + S* biomass composite with silica, *MBM + S* milled biomass composite with silica, *BM + Z* biomass composite with zeolite, *MBM + Z* milled biomass composite with zeolite, *BC* biochar, *MBC* milled biochar, *BC + S* biochar composite with silica, *MBC + S* milled biochar composite with silica, *BC + Z* biochar composite with zeolite, *MBC + Z* milled biochar composite with zeolite

Average effective particle size (EPS) was greatly reduced in biochars compared to biomass as a consequence of pyrolysis (Fig. 2b). Particularly, the biochar composites with silica and zeolite exhibited large EPS than biochar alone. This could possibly be due to some interactions of biochar particles with silica and zeolite minerals. As pyrolysis goes on, CO_2 starts evolving from the biomass; therefore, sodium in zeolite may bound to O_2-containing functional groups of biochar to form a stable ionic metal phenoxides. Similarly, silica interacts with biochar to form complexed structured minerals such as feldspathoids (Joseph et al. 2013). These organo-minerals complexes resulted in higher average effective particle size of silica and zeolite composites compared to the biochar.

SEM and FTIR analyses

Surface morphology of the date palm waste biomass and derived biochar composites analyzed by SEM is shown in Fig. 3. Pyrolysis increased the porosity and created channels in the biochars by volatilization of organic matter (Usman et al. 2015). As volatiles escaped from the biomass during thermalization, it created new small pores. However, surface coverage and pore blockage with silica and zeolite were visible in the silica and zeolite composited biochars (Fig. 3g, h, k, l). The smaller mineral particles penetrated into the channels, thereby blocking the pores and decreased surface area eventually.

FTIR spectra of date palm tree waste biomass and derived biochar composites in the range of 600–4000 cm^{-1} are shown in Fig. 4. A band at 693 cm^{-1} was designated as Si–O, which was sharp in raw silica sample, while peak intensity decreased in silica composited biomass and biochars. A band of Si–

O at 779 cm^{-1} was present in all the materials with little shifts in band location. A band at 1089 cm^{-1} presented in all the samples was due to C–O–C stretches (polysaccharide cellulose, which became sharp during the pyrolysis process) and TO_4 (tetrahedral) of Al–Si, which indicated the presence of clinoptilolite (Na, K, Ca)$_{2–3}Al_3(Al,Si)_2Si_{13}O_{36}·12H_2O$). A broad band around 3300 cm^{-1} in biomass (BM and MBM) confirmed the presence of –OH stretches of H-bounded water molecules and other volatile functional groups, which were lost during pyrolysis and disappeared in the biochars (BC and MBC) (Fig. 4a). These bands were reduced in silica and zeolite composited biomass due to drying during the impregnation process (Fig. 4b, c). Bands at 2920 and 2849 cm^{-1} in biomass were assigned as O–H and aliphatic C–H stretching, respectively, representing hemicellulose and cellulose. No band detection at 2900-3200 cm^{-1} in biochar materials suggested the removal of aliphatic compounds and polar functional groups during pyrolysis (Usman et al. 2015; Jouiad et al. 2015). A band at 1607 cm^{-1} was due to –COOH in all biomass materials indicated the presence of carboxylic groups (such as ketones, esters and carboxyl) associated with hemicellulose. These groups eliminated with thermal treatment of biomass. A band with high absorbance at 1055 cm^{-1} in all the materials designated as C–O–C stretches confirmed the presence of polysaccharide cellulose, which became sharp during the pyrolysis process. Shifts in bands location due to complexation in composites are shown in Table S2. A band is credited as Si–O was shifted from 693 cm^{-1} in raw silica to 691 cm^{-1} in BM + S and MBM + S, while it again was shifted to 693 cm^{-1} in BC + S and MBC + S. Likewise, Si–O band at 779 cm^{-1} in raw silica was shifted to 775 and 777 cm^{-1} in BM + S and MBM + S, respectively, and it shifted again to 779 cm^{-1} in BC + S and MBC + S. The band designated as clinoptilolite at 1034 cm^{-1} in zeolite did not change its location in BM + Z and MBM + Z, while it shifted to 1056 cm^{-1} in BC + Z and MBC + Z. These shifts in bands of FTIR spectra reflect that some interactions and complexation have taken place between minerals and biochar in composites. These results showed

Fig. 3 Scanning electron microscope (SEM) images of date palm tree rachis waste biomass and its derived biochars. **a** Biomass (BM), **b** milled biomass (MBM), **c** biochar (BC), (**d**) milled biochar (MBC), (**e**) biomass composite with silica (BM+S), (**f**) milled biomass composite with silica (MBM+S), (**g**) biochar composite with silica (BC+S), (**h**) milled biochar composite with silica (MBC+S), (**i**) biomass composite with zeolite (BM+Z), (**j**) milled biomass composite with zeolite (MBM+Z), (**k**) biochar composite with zeolite (BC+Z), and (**l**) milled biochar composite with zeolite (MBC+Z)

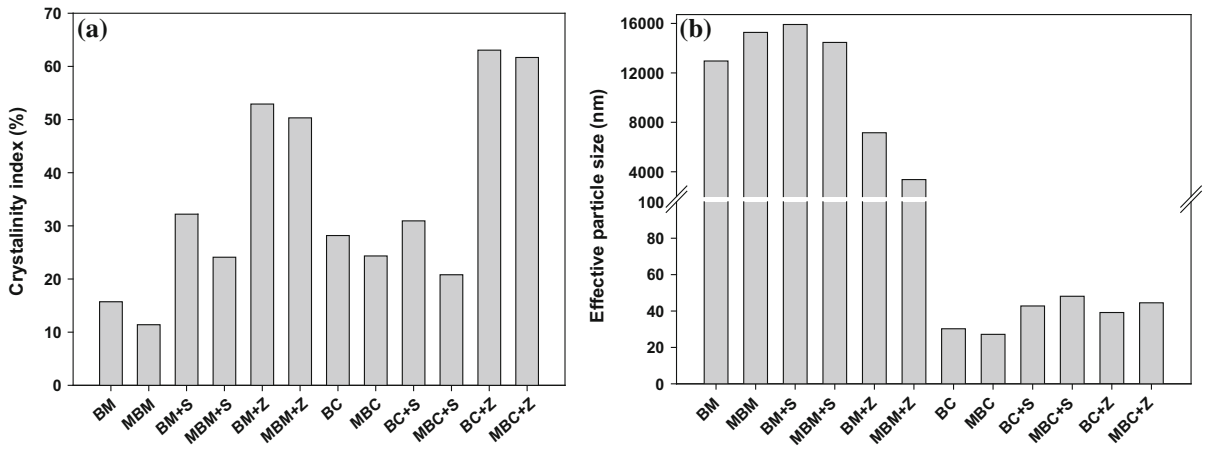

Fig. 2 Crystallinity index (**a**) and average effective particle size (**b**) of date palm tree rachis waste biomass and its derived biochars. (BM, biomass; MBM, milled biomass; BM + S, biomass composite with silica; MBM + S, milled biomass composite with silica; BM + Z, biomass composite with zeolite; MBM + Z, milled biomass composite with zeolite; BC, biochar; MBC, milled biochar; BC + S, biochar composite with silica; MBC + S, milled biochar composite with silica; BC + Z, biochar composite with zeolite; MBC + Z, milled biochar composite with zeolite)

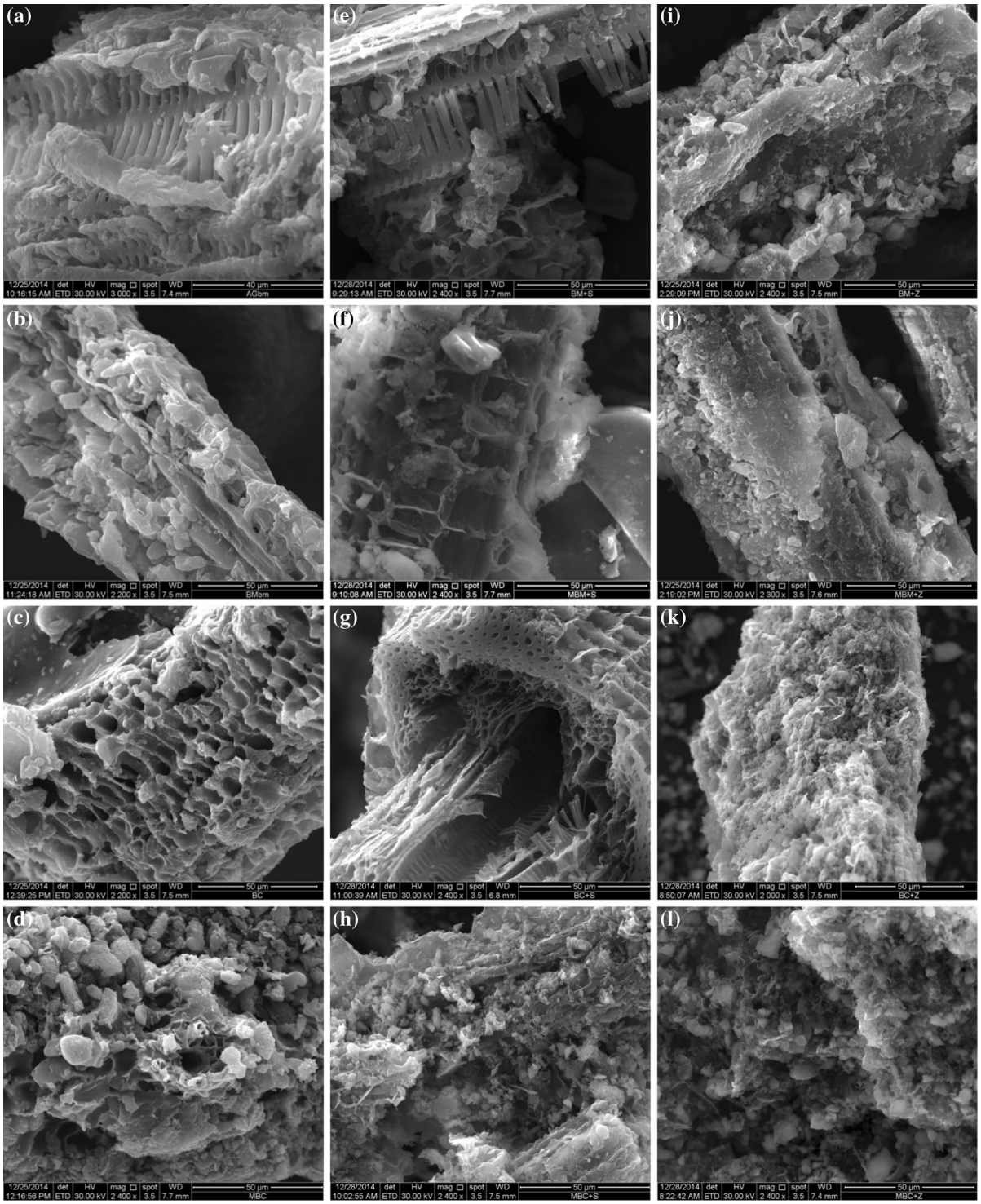

changes in functional groups of the date palm waste biochar with mechanochemical treatments. This information can further help to predict the effect of silica/clay impregnation/enrichment to biochar on sorption efficiencies of biochars for various contaminants.

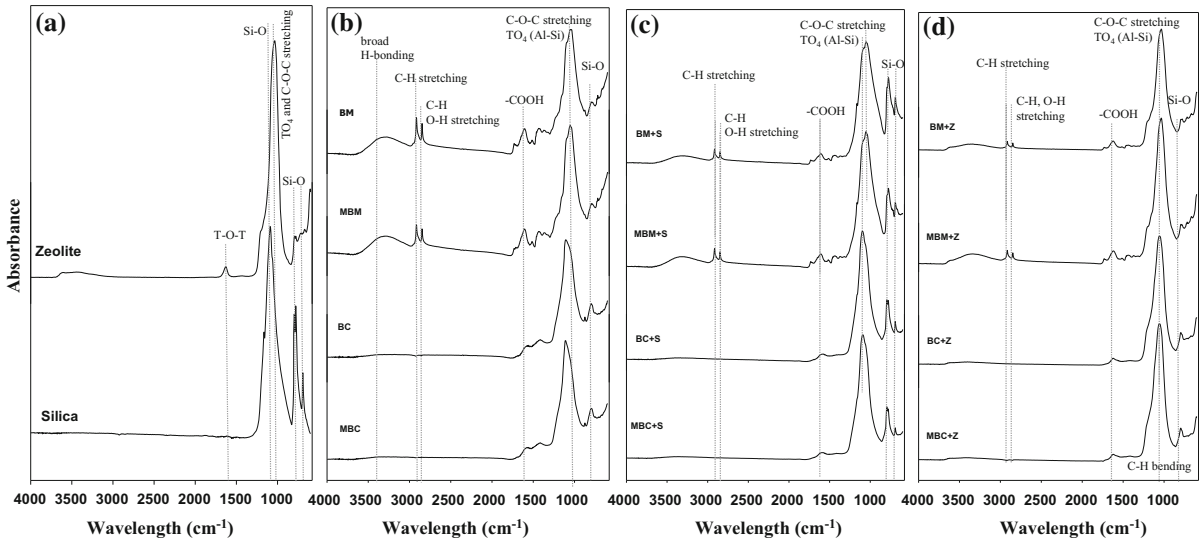

Fig. 4 FTIR spectra of (**a**) pristine zeolite and silica powders, **b** date palm tree rachis waste biomass and its derived biochars, **c** silica composited biomass and its derived biochars, and **d** zeolite composited biomass and its derived biochars. (BM, biomass; MBM, milled biomass; BM + S, biomass composite with silica; MBM + S, milled biomass composite with silica; BM + Z, biomass composite with zeolite; MBM + Z, milled biomass composite with zeolite; BC, biochar; MBC, milled biochar; BC + S, biochar composite with silica; MBC + S, milled biochar composite with silica; BC + Z, biochar composite with zeolite; MBC + Z, milled biochar composite with zeolite)

Elemental composition

Elemental composition of the date palm leaves waste biomass and derived composites are shown in Table 3. Thermal treatment increased total C contents in biochars and their composites compared to biomass and their composites. The increase in C contents with pyrolysis could be due to increased degree of carbonization. Highest C contents increase was observed in silica composited biochar compared to silica composited biomass. An increase of 57% in BC + S was observed as compared to BM + S and 48% in MBC + S compared with MBM + S. This high C percentage in silica composited biochars could be attributed to the strong and stable bonding of C–Si which was resistant to the thermal treatments during pyrolysis (Liu et al. 2006). Reduction in H contents was 65.5% in BC compared to BM, but interestingly it increased in the composites of zeolite and silica with pyrolysis, that could be due to the bonding of H with silica and zeolite minerals (except MBC + S). Total N and O contents decreased with thermalization of the biomass. Nitrogen was mostly lost with pyrolysis in all the composites except BC + S. The maximum

Table 3 Elemental composition and their molar ratios of date palm tree waste biomass and its derived biochars

	C (%)	H (%)	N (%)	O (%)	O/C	H/C
BM	48.46	9.73	3.20	38.61	0.60	2.39
MBM	41.21	7.23	2.89	48.67	0.89	2.09
BM + S	32.59	4.62	2.45	60.33	1.39	1.69
MBM + S	38.64	6.48	2.86	52.01	1.01	2.00
BM + Z	38.20	7.71	3.12	50.97	1.00	2.40
MBM + Z	57.54	7.63	3.34	31.48	0.41	1.58
BC	76.23	3.36	0.00	20.40	0.20	0.53
MBC	75.59	4.89	0.00	19.51	0.19	0.77
BC + S	75.86	9.44	3.57	11.13	0.11	1.48
MBC + S	74.64	1.35	0.00	24.01	0.24	0.22
BC + Z	56.15	9.14	0.00	34.71	0.46	1.94
MBC + Z	73.03	13.36	0.00	13.61	0.14	2.18

BM biomass, *MBM* milled biomass, *BM + S* biomass composite with silica, *MBM + S* milled biomass composite with silica, *BM + Z* biomass composite with zeolite, *MBM + Z* milled biomass composite with zeolite, *BC* biochar, *MBC* milled biochar, *BC + S* biochar composite with silica, *MBC + S* milled biochar composite with silica, *BC + Z* biochar composite with zeolite, *MBC + Z* milled biochar composite with zeolite

reduction in O was observed in BC + S (81.5%) while minimum in BC + Z (31.9%). Reduction in O and N contents with pyrolysis could be due to loss of O-containing functional groups by dehydration, depolymerization and volatilization (Al-wabel et al. 2013; Ahmad et al. 2014b). Surface polarity (indicated by O/C molar ratio) decreased as a result of pyrolysis indicating a decrease in hydrophobicity of biochars. Biochar composites with silica and zeolite did not show any remarkable effect on biochar's surface polarity, except in the case of BC + Z. This high surface polarity of BC + Z composite (0.46) could be due to the potential of the mineral to prevent the removal of polar functional groups (Qiu et al. 2014). Low H/C values for BCs compared to BM and mineral composites indicated high aromaticity and reactivity. Specifically, the biochar composites with silica and zeolite minerals showed less aromaticity or reactivity (H/C ratio >1.0; except MBC + S) than BC, which could be associated with the blockage of char's active sites with mineral particles (Odeh 2015). Higher aromaticity and lower polarity of silica composited biochar might be due to the formation of various Si–C polytypes structures through the layers of CSi_4 or SiC_4 in polar framework and formation of non-hydrolyzable pendant organic chains with Si–C bonding (Izhevskyil et al. 2000; Deya and Airoldi 2008).

Effect on ball milling

Milling can significantly reduce the particle size of biomass, thus enhancing thermal decomposition. All biochars derived from milled biomass showed less yield (ranging from 19.13 to 23.08%) compared with non-milled biomass-derived biochars. This could be attributed to the greater loss of volatile compounds due to greater thermal exposure of small sized particles of milled biomass. Moreover, size reduction by milling boosted thermal degradation of lingo-cellulosic material resulting in a lower yield of milled BCs (Antal and Grönli 2003). Reduction in yield of milled biochars was further related to high mobile/volatile matter in milled biomass. Ball-milled composites showed higher CEC values as compared to non-milled composites, which might be due to smaller particle size and amorphous nature of the milled composites. An inverse relationship between particle size and CEC has been previously reported (Altland et al. 2014).

Ball milling can break the crystalline structure of cellulose and can transform it into an amorphous material. This was confirmed by calculating the crystallinity indices (CrI) for each material based on the XRD peak intensities as shown in Fig. 2a. Reduction in CrI of milled biomass and biochars indicated that ball milling has broken down the crystalline structure of cellulose in the biomass, making it more amorphous (Murillo et al. 2014), which can also be seen by reduced intensities of peaks in XRD patterns (Fig. 1). In biomass materials, maximum crystallinity reduction (27.55%) was depicted in MBM, followed by MBM + S (25.17%) and MBM + Z (4.88%). Comparing crystallinity reduction of biochars, maximum reduction was observed in MBC + S (32.76%), followed by MBC (13.59%) and MBC + Z (2.19%). The decrease in cellulose crystallinity was also evident from FTIR spectral peak at a wavelength of 1055 cm^{-1}, which was attributed to crystalline cellulose. The disintegration of cellulose crystallinity due to milling reduced the peak breadth of C–O stretching vibrations. Smaller particle size and reduced crystallinity led to a more defined peak in milled biomass and biochars (Fig. 1a).

Milling resulted in 12.54 and 13.74% increase in BET surface area of BMC + S and MBC + Z composites, which could be related to their poor crystallinity caused by milling. Disordered or imperfectly stacked crystals in the milled biochar composites may have given rise to the high surface area (Murray and Lyons 1959). Likewise, the pore size of milled biochars and their composites was slightly higher than non-milled precursors. To see the impact of milling on particle size, EPS was calculated from BET surface area data. With ball milling, due to breaking down of crystalline cellulose, the biochar composites attain higher surface charge and more amorphous nature. Due to more charge on broken edges, milled biochar composites formed more strong complexes of biochar with silica or zeolite making particles aggregates with larger EPS values. This physical disintegration and particles aggregation effect of milling was also observed in SEM images (Fig. 3).

Carbon stability

Contents of labile C (potentially unstable), non-labile C (potentially recalcitrant or fixed) and active organic C are shown in Fig. S1. Pyrolysis significantly decreased the active organic C in biochars (76.57% reduction) compared to biomass. Likewise, the labile C fraction decreased and non-labile C fraction increased as a result of pyrolysis, indicating the effectiveness of pyrolyzing the biomass to form a C stable biochar. Converting the easily decomposable biomass to stable biochar via pyrolysis is well known to sequester C and mitigate CO_2 emissions into the atmosphere (Lehmann 2007). Mineral composites of biochar (silica and zeolite composited biochars) showed relatively high labile C fraction than BC, which could be due to physical protection of organic matter by minerals occlusion (Greathouse et al. 2014). Non-labile C (potentially stable) increased in biochars compared with biomass due to dehydration and increased degree of aromaticity. The commonly used van Krevelen plot between molar H/C and O/C ratios to estimate recalcitrance of biochar is shown in Fig. 5. With pyrolysis, date palm biomass converted into smaller dissociation products through dehydration and depolymerization (Keiluweit et al. 2010). Reduction in molar ratios of H/C and O/C suggested lower polarity and a higher degree of aromaticity, subsequently resulting in higher stability of the biochars (Usman et al. 2015). In the van Krevelen plot, MBC + S was closest to the origin, representing minimum O/C and H/C ratios among all the materials. MBC + S and BC + S showed minimum values of H/C (0.22) and O/C (0.11) molar ratios (Table 3) suggesting higher aromaticity and lower polarity, respectively, among all the materials, indicating higher recalcitrance and C stability. Generally, an O/C molar ratio less than 0.2 predicts a minimum half-life of 1000 years for the given biochar material (Spokas 2010). Lowest O/C molar ratio of BC + S (0.11) among all other synthesized materials in the current study suggested the longest half-life of silica composited biochar (more than 1000 years). O/C molar ratio does not only account for pyrolysis temperature but also is a function of composition and type of pristine material and post-pyrolysis conditioning; therefore, it is the strongest indicator to predict the stability of biochar compared to other pyrolysis parameters such as temperature, volatile matter analysis and type of the feedstock (Spokas 2010).

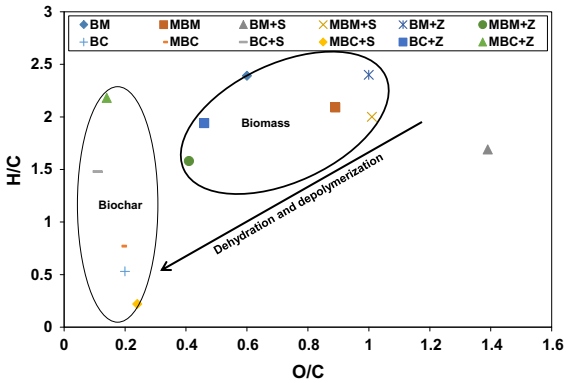

Fig. 5 van Krevelen diagram of elemental ratios of H/C and O/C for date palm tree rachis waste biomass and its derived biochars. (BM, biomass; MBM, milled biomass; BM + S, biomass composite with silica; MBM + S, milled biomass composite with silica; BM + Z, biomass composite with zeolite; MBM + Z, milled biomass composite with zeolite; BC, biochar; MBC, milled biochar; BC + S, biochar composite with silica; MBC + S, milled biochar composite with silica; BC + Z, biochar composite with zeolite; MBC + Z, milled biochar composite with zeolite)

Recalcitrance index (R_{50})

Due to highly condensed aromatic structure, biochar generally considered as thermally, chemically, physically and biologically recalcitrant. Potential of biochar to resist thermal, physical and chemical degradation (referred as recalcitrance) is considered as a crucial factor for C sequestration in soil. Biochar stability is largely dependent on aromatic carbon structure and the formation of organometallic complexes. Biochar C has greater recalcitrance potential than that of the feedstock due to enhanced aromaticity; however, C recalcitrance and stability in the soil after biochar addition varies depending on feedstock type and composition, soil texture, structure and other environmental factors. Therefore, an index is needed to estimate recalcitrance of biochar in relation to graphite, which is considered as one of the most stable C forms (Windeatt et al. 2014). Harvey et al. (2012) developed a new recalcitrance index using TGA thermograms which are noted as R_{50} to predict the recalcitrance potential of a typical biochar.

TGA thermogravimetric analysis was used to test the long-term stability of biochar composites

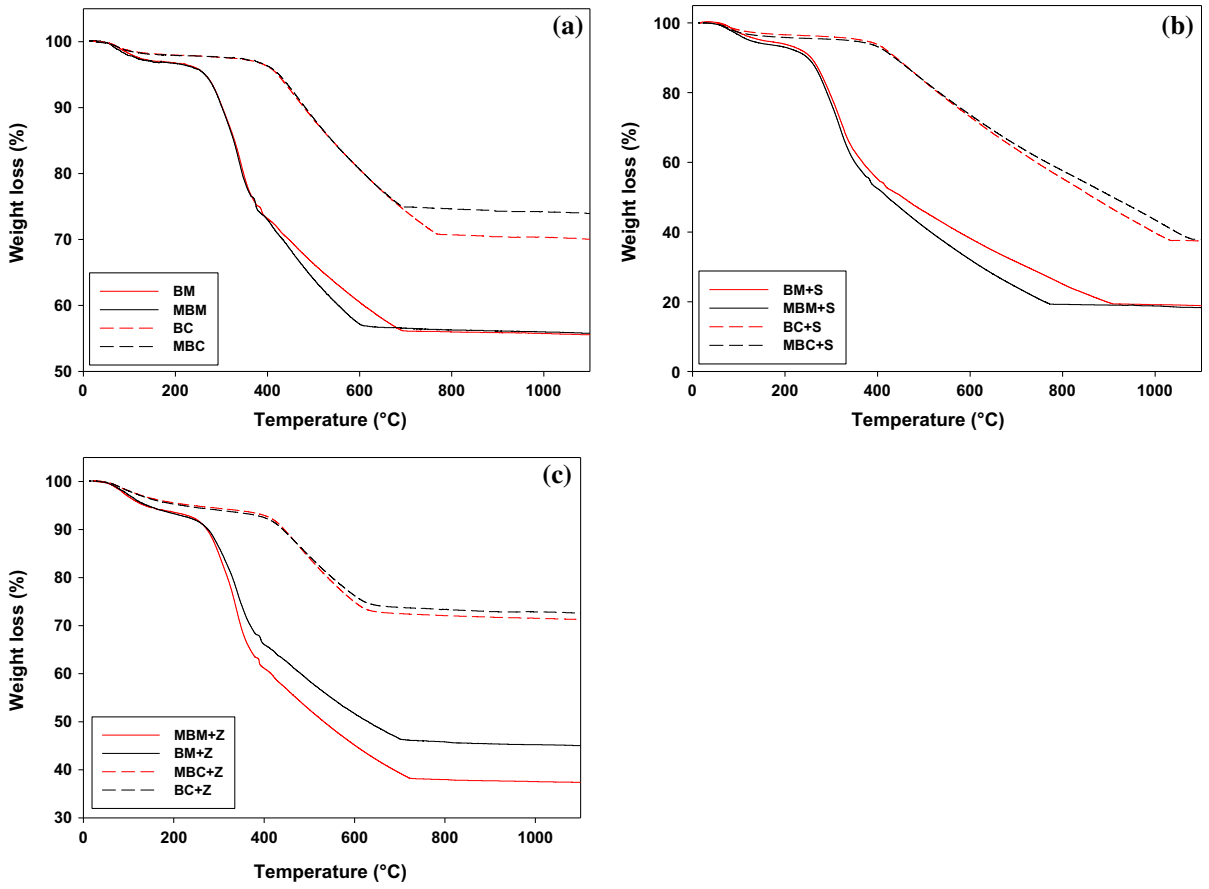

Fig. 6 Thermogravimetric analysis (TGA) of date palm tree rachis waste biomass and its derived biochars. **a** Biomass (BM), milled biomass (MBM), biochar (BC), milled biochar (MBC); **b** biomass composite with silica (BM + S), milled biomass composite with silica (MBM + S), biochar composite with silica (BC + S), milled biochar composite with silica (MBC + S); and **c** biomass composite with zeolite (BM + Z), milled biomass composite with zeolite (MBM + Z), biochar composite with zeolite (BC + Z), milled biochar composite with zeolite (MBC + Z)

synthesized in this study. Thermograms of a typical TGA-DTG analysis are shown in Fig. 6. Three general regions of weight loss were identified on the thermograms, (i) around 200 °C due to loss of non-structural free water from pores and surface of the materials (Yang et al. 2007; Scheirs et al. 2001), (ii) around 300 °C for biomass and 400 °C for biochars due to thermal degradation of hemicellulose and cellulosic compounds (Yang et al. 2007) and (iii) around 650–1050 °C in different materials due to lignin degradation. Biomass thermally decomposed earlier than that of produced biochars because of thermal instability. TGA thermograms were corrected for moisture and ash contents (including silica and zeolite) to calculate R_{50}. Moisture and ash corrected TGA thermograms are shown in Fig. 7. Depending upon R_{50} values, biochars can be divided into three categories (Harvey et al. 2012):

1. $R_{50} \geq 0.7$ = Highly recalcitrant
2. $0.7 > R_{50} \geq 0.5$ = Minimal degradable
3. $R_{50} < 0.5$ = Highly degradable

All the biomass materials in our research showed R_{50} values around 0.4 suggesting that these belong to class 3, i.e., highly degradable (Table 4). Silica composited biochars (BC + S and MBC + S) were categorized in class 1 with R_{50} of 0.75 and 0.76, respectively, suggesting their high recalcitrance potential. Biochars (BC and MBC) and zeolite composited biochars (BC + Z and MBC + Z) were comparable in their recalcitrance potential as they fall in class 2 which is minimally degradable with R_{50}

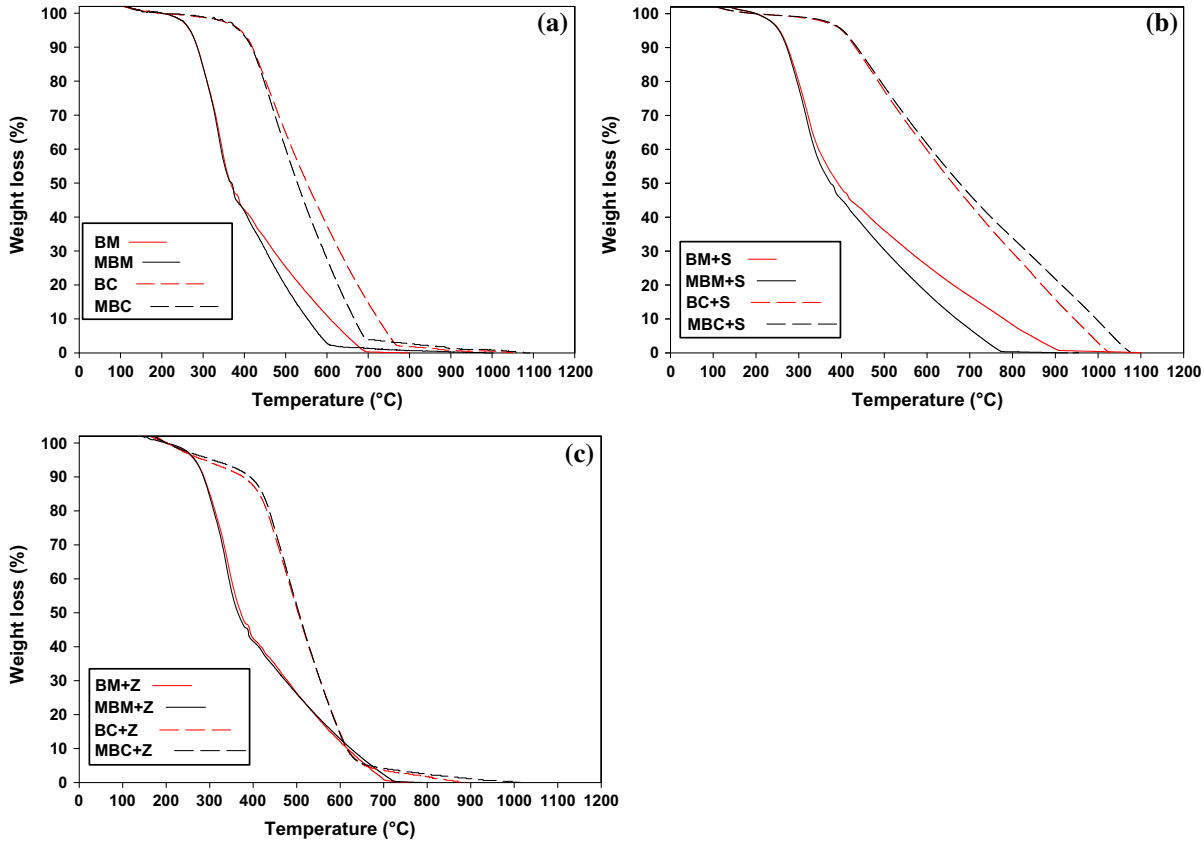

Fig. 7 Moisture, ash, silica and zeolite corrected TGA thermograms of date palm tree rachis waste biomass and its derived biochars. **a** Biomass (BM), milled biomass (MBM), biochar (BC), milled biochar (MBC); **b** biomass composite with silica (BM + S), milled biomass composite with silica (MBM + S), biochar composite with silica (BC + S), milled biochar composite with silica (MBC + S); and **c** biomass composite with zeolite (BM + Z), milled biomass composite with zeolite (MBM + Z), biochar composite with zeolite (BC + Z), milled biochar composite with zeolite (MBC + Z)

values below 0.7 but higher than 0.5. Increased R_{50} in silica composited biochars could be attributed to the probable protection of C by silica particles which may be controlled through pyrolysis process (Guo and Chen 2014). Higher R_{50} values of silica composited biochars predict higher recalcitrance/stability of BC + S and MBC + S due to specific interactions of Si particles with biochar matrix. Therefore, it can be stated that the presence of Si particles in biochar matrix was also an important factor other than aromaticity to predict long-term stability of biochar.

Recalcitrance index (R_{50}) does not tell about the precise timescale for C sequestration, rather gives a range of recalcitrance relevant to graphite (highly stable C form). Therefore, carbon sequestration potential (*CS*) was calculated using R_{50} and an equation given by Zhao et al. (2013), which stated that C sequestration would be in the range of 100-1000 years (Table 4). In our study, biochars (BC and MBC) and zeolite composited biochars (BC + Z and MBC + Z) exhibited *CS* in the range of 30.26–43.19%, while silica composited biochars shown highest *CS* percentage of up to 95.59% (BC + S) and 64.17% (MBC + S). As *CS* depends upon (i) the C contents (%) before and after pyrolysis, (ii) R_{50} and (iii) yield (%) of the biochar, increased *CS* percentage was due to higher R_{50} values as well as higher yield of silica composited biochar due to the presence of thermally resistant Si.

Probable half-life ($t_{1/2}$) of C was estimated with a theoretical model (supplementary data) using R_{50} values in optimal laboratory conditions without considering the effect of mineral contents (Fig. S2). The half-life for the C in composited biomass ranged

Table 4 Temperature corresponding to 50% weight loss of water and ash-free composites (T_{50}), recalcitrant index (R_{50}) and carbon sequestration potential (CS) of date palm tree leaves waste biomass and its derived biochars

Sample	T_{50}	R_{50}	CS (%)
BM	391.62	0.44	–
MBM	374.32	0.42	–
BM + S	366.49	0.41	–
MBM + S	369.13	0.42	–
BM + Z	371.54	0.42	–
MBM + Z	364.69	0.41	–
BC	551.90	0.62	40.49
MBC	529.04	0.60	34.80
BC + S	660.37	0.75	95.59
MBC + S	675.79	0.76	64.17
BC + Z	503.28	0.57	43.19
MBC + Z	505.06	0.57	30.26
Z	306.14	0.346	–
S	519.81	0.587	–
Graphite	886.00	1.000	–

BM biomass, *MBM* milled biomass, *BM + S* biomass composite with silica, *MBM + S* milled biomass composite with silica, *BM + Z* biomass composite with zeolite, *MBM + Z* milled biomass composite with zeolite, *BC* biochar, *MBC* milled biochar, *BC + S* biochar composite with silica, *MBC + S* milled biochar composite with silica, *BC + Z* biochar composite with zeolite, *MBC + Z* milled biochar composite with zeolite

between 71 and 185 years, while for the composites of biochars, it ranged 1×10^4 to 5×10^6 years. MBC + S and BC + S showed highest C half-life of 5×10^6 and 3×10^6, respectively, indicating highly recalcitrant nature of the biochars composited with silica. This was due to Si–C bonding and Si encapsulation as discussed above. These results are in agreement with the findings of Zimmerman et al. (2011), who suggested the half-lives of biochars in the range of 10^2–10^7 years through modeling of laboratory incubation trials results. Due to the long half-life of biochar, the rate of transfer of organic C from the biochar to CO_2 in the atmosphere is very slow, which results in higher C sequestration potential. Through C dating, Lal (2003) found some biochar materials (charcoal) more than 1500 years old but still were stable having permanent forms of C sequestration. Spokas (2010) suggested a half-life of at least 1000 years for the materials having O/C molar ratios <0.2. Silica composited biochar in this study exhibited O/C molar ratio of 0.11 suggesting a half-life of more than 1000 years (Table 3), which is in accordance with the results obtained from theoretical model for half-life calculations.

Higher half-life and recalcitrance potential (R_{50}) of silica composited biochars might be due to a specific organo-mineral complex formed during synthesis of silica composited biochars. When a feedstock with silica particles in its composition is pyrolyzed, silica particle may affect C arrangements and structural composition by producing a Si–C coupling system in biochar matrix. Formation of Si–C coupling system may have escalated a dense structure resulting in the production of Si-encapsulated C (Guo and Chen 2014; Xiao et al. 2014). Si encapsulations might have prevented thermal degradation of C by protecting C particles in the inner core, subsequently increasing the stability of the biochar. Oxidation of the biochar begins at the surfaces of the matrix, and if the outer surface contains some strong encapsulation/core, oxidation cannot penetrate into the inner core even in very old biochars (Cheng et al. 2006; Liang et al. 2006). Additionally, if applied to soil, other organics may adsorb on the surface of the biochar, which mineralized first protecting the encapsulated C in the inner core of the original structure (Lehmann et al. 2005; Liang et al. 2006). In this study, silica may have encapsulated the C particles by protecting it in the inner core. Due to Si encapsulation, C particles were protected with covering of thermally resistant Si particles; therefore, silica composited biochars decomposed at a higher temperature compared to other biochars as confirmed from TGA thermograms (Fig. 6). Xiao et al. (2014) reported a mutual protective interaction of C and Si particle within the biochar matrix due to structure and morphology of Si–C complex. Silica protected C particles from decomposition resulting in higher C stability, while C particle reduced the dissolution of Si. These mutual protective interactions have eventually resulted in higher recalcitrance/stability of silica composited biochars. Due to the strong interaction between Si and C, silica composited biochars can be used as a potential strategy to sequester atmospheric C in soil organic carbon pool for longer times. These composites can also be used as low-cost slow-release Si fertilizer in less-fertile Si-deficient soils and for climate change mitigation due to strong

affinity of silica for CO_2. However, further studies are required to explore the molecular composition of Si–BC complex at nanoscale level and half-life of biochar in association with silica at field levels in real environmental situations.

Conclusions

Engineered biochar composites with silica and zeolite were synthesized via mechanochemical treatments to investigate the variations in physicochemical characteristics, recalcitrance potential and carbon stability of synthesized composites. Structural, morphological and chemical analyses indicated variations in the characteristics of virgin and engineered biochars. Silica composited biochars exhibited higher recalcitrance indices ($R_{50} > 0.7$) and C sequestration potentials (64.17–95.59%). Silica particles in biochar matrix affected C arrangement and structural composition. Due to ball milling, silica converted to amorphous material which escalated a dense structure when blended with the biochar, producing C–Si bounding resulting in encapsulation of C particles by Si. Si encapsulation prevented thermal degradation of C particles subsequently increasing its stability. Therefore, it can be stated that Si protection is also an important factor other than the aromaticity, for the stability of biochar. Silica composited biochars can be used to sequester soil organic C pool for a longer time when applied as a soil amendment. In future, silica composited biochars can be investigated for their efficiency as low-cost slow-release Si fertilizer in less-fertile Si-deficient soils, for climate change mitigation due to high capture affinity of silica for CO_2 and for contaminants removal from the environmental compartments, as a result of the increased adsorption sites by introducing silica particles on biochar matrix.

Acknowledgements The authors extend their appreciation to the Deanship of Scientific Research, King Saud University, for funding this work through the international research group project IRG-14-14.

References

Ahmad, M., Moon, D. H., Vithanage, M., Koutsospyros, A., Lee, S. S., Yang, J. E., et al. (2014a). Production and use of biochar from buffalo-weed (*Ambrosia trifida* L.) for trichloroethylene removal from water. *Journal of Chemical Technology and Biotechnology, 89,* 150–157.

Ahmad, M., Rajapaksha, A. U., Lim, J. E., Zhang, M., Bolan, M., Mohan, D., et al. (2014b). Biochar as a sorbent for contaminant management in soil and water: A review. *Chemosphere, 99,* 19–33.

Altland, J. E., Locke, J. C., & Krause, C. R. (2014). Influence of pine bark particle size and pH on cation exchange capacity. *HortTechnology, 24,* 554–559.

Al-Wabel, M. I., Al-Omran, A., El-Naggar, A. H., Nadeem, M., & Usman, A. R. A. (2013). Pyrolysis temperature induced changes in characteristics and chemical composition of biochar produced from conocarpus wastes. *Bioresource Technology, 131,* 374–379.

American Society for Testing and Materials (ASTM). (1989). Standard Methods for Chemical Analysis of Wood Charcoal, ASTM D1762-84, Philadelphia, PA, USA.

Antal, J. M. J., & Grönli, M. (2003). The art science, and technology of charcoal production. *Industrial and Engineering Chemistry Research, 42,* 1619–1640.

Bilgic, C. (2005). Investigation of the factors affecting organic cation adsorption on some silicate minerals. *Journal of Colloid and Interface Science, 281,* 33–38.

Blair, G. J., Lefroy, R. D. B., & Lisle, L. (1995). Soil carbon fractions based on their degree of oxidation, and the development of a carbon management index for agricultural systems. *Australian Journal of Agricultural Research, 46,* 1459–1466.

Bonenfant, D., Kharoune, M., Niquette, P., Mimeault, M., & Hausler, R. (2008). Advances in principal factors influencing carbon dioxide adsorption on zeolite. *Science and Technology of Advanced Materials, 9,* 1–7.

Cheng, C. H., Lehmann, J., Thies, J. E., Burton, S. D., & Engelhard, M. H. (2006). Oxidation of black carbon by biotic and abiotic processes. *Organic Geochemistry, 37,* 1477–1488.

Deya, R. D., & Airoldi, C. (2008). Designed pendant chain covalently bonded to silica gel for cation removal. *Journal of Hazardous Materials, 156,* 95–101.

Fosso-kankeu, E., Waanders, F. B., Steyn, F. W. (2015). The preparation and characterization of clay-biochar composites for the removal of metal pollutants. In *7th International Conference on latest Trends in Engineering and Technology (ICLTET'2015)*, At Irene Pretoria South Africa, Volume: ISBN 978-93-84422-58-2. pp. 53–57.

Fowles, M. (2007). Black carbon sequestration as an alternative to bioenergy. *Biomass and Bioenergy, 31,* 426–432.

Greathouse, J. A., Johnson, K. L., & Greenwell, H. C. (2014). Interaction of natural organic matter with layered minerals: Recent developments in computational methods at the nanoscale. *Minerals, 4,* 519–540.

Guo, J., & Chen, B. (2014). Insights on the molecular mechanism for the recalcitrance of biochars: Interactive effects of carbon and silicon components. *Environmental Science and Technology, 48,* 9103–9112.

Gurses, A., Dogar, C., Yalcin, M., Acikyildiz, M., Bayrak, R., & Karaca, S. (2006). The adsorption kinetics of the cationic dye, methylene blue, onto clay. *Journal of Hazardous Materials, 131,* 217–228.

Harvey, O. R., Kuo, L. J., Zimmerman, A. R., Louchouarn, P., Amonette, J. E., & Herbert, B. E. (2012). An index-based

approach to assessing recalcitrance and soil carbon sequestration potential of engineered black carbons (biochars). *Environmental Science and Technology, 46,* 1415–1421.

Hendershot, W. H., Lalande, H., & Duquette, M. (2008). Ion exchange and exchangeable cations. In M. R. Carter & E. G. Gregorich (Eds.), *Soil sampling and methods of analysis* (2nd ed., pp. 197–206). Boca Raton, FL: CRC Press.

Inyang, M., Gao, B., Pullammanappallil, P., Ding, W., & Zimmerman, A. R. (2010). Biochar from anaerobically digested sugarcane bagasse. *Bioresource Technology, 101,* 8868–8872.

Izhevskyil, V. A., Genova, L. A., Bressiani, J. C., & Bressiani, A. H. A. (2000). Review article: Silicon carbide. Structure, properties and processing. *Cerâmica, 46,* 297. doi:10.1590/S0366-69132000000100002.

Joseph, S. D., Camps-Arbestain, M., Lin, Y., Munroe, P., Chia, C. H., Hook, J., et al. (2010). An investigation into the reactions of biochar in soil. *Australian Journal of Soil Research, 48,* 501–515.

Joseph, S., Graber, E. R., Chia, C., Munroe, P., Donne, S., Thomas, T., et al. (2013). Shifting paradigms: Development of high-efficiency biochar fertilizers based on nanostructures and soluble components. *Carbon Management, 4,* 323–343.

Jouiad, M., Al-Nofeli, N., Khalifa, N., Benyettou, F., & Yousef, L. F. (2015). Characteristics of slow pyrolysis biochars produced from rhodes grass and fronds of edible date palm. *Journal of Analytical and Applied Pyrolysis, 111,* 183–190.

Keiluweit, M., Nico, P. S., Johnson, M. G., & Kleber, M. (2010). Dynamic molecular structure of plant biomass-derived black carbon (biochar). *Environmental Science and Technology, 44,* 1247–1253.

Kuzyakov, Y., Subbotina, I., Chen, H., Bogomolova, I., & Xu, X. (2009). Black carbon decomposition and incorporation into soil microbial biomass estimated by ^{14}C labeling. *Soil Biology & Biochemistry, 41,* 210–219.

Laird, D. A. (2008). The charcoal vision: A win win win scenario for simultaneously producing bioenergy, permanently sequestering carbon, while improving soil and water quality. *Agronomy Journal, 100,* 178–181.

Lal, R. (2003). Global potential of soil carbon sequestration to mitigate the greenhouse effect. *Critical Reviews in Plant Sciences, 22,* 151–184.

Lal, R. (2004). Soil carbon sequestration impacts on global climate change and food security. Soils—the final Frontier. *Science, 304,* 1623–1627.

Lehmann, J. (2007). A handful of carbon. *Nature, 447,* 143–144.

Lehmann, J., Gaunt, J., & Rondon, M. (2006). Bio-char sequestration in terrestrial ecosystems—A review. *Mitigation and Adaptation Strategies for Global Change, 11,* 403–427.

Lehmann, D. J., & Joseph, S. (2009). *Biochar for environmental management: Science and technology London*. Sterling, VA: Earthscans.

Lehmann, J., Liang, B. Q., Solomon, D., Lerotic, M., Luizão, F., Kinyangi, J., et al. (2005). Nearedge X-ray absorption fine structure (NEXAFS) spectroscopy for mapping nano-scale distribution of organic carbon forms in soil: Application to black carbon particles. *Global Biogeochemical Cycles, 19,* GB1013. doi:10.1029/2004GB002435.

Lenton, T. M., & Vaughan, N. E. (2009). The radiative forcing potential of different climate geoengineering options. *Atmospheric Chemistry and Physics Discussions, 9,* 2559–2608.

Liang, B., Lehmann, J., Solomon, D., Kinyangi, J., Grossman, J., O'Neill, B., et al. (2006). Black carbon increases cation exchange capacity in soils. *Soil Science Society of America Journal, 70,* 1719–1730.

Liu, R., Shi, Y., Wan, Y., Meng, Y., Zhang, F., Gu, D., et al. (2006). Triconstituent co-assembly to ordered mesostructured polymer-silica and carbon-silica nanocomposites and large-pore mesoporous carbons with high surface areas. *Journal of the American Chemical Society, 128,* 11652–11662.

Lowell, S., Shields, J. E., Thomas, M. A., & Thommes, M. (2004). Characterization of porous solids and powders: Surface area, pore size and density. In B. Scarlett (Ed.), *Practicle Technology series*. The Netherlands: Kluwer Academic Publishers.

Mukherjee, A., Zimmerman, A. R., & Harris, W. (2011). Surface chemistry variations among a series of laboratory-produced biochars. *Geoderma, 163,* 247–255.

Murillo, J. D., Ware, E. A., & Biernacki, J. J. (2014). Characterization of milling effects on the physical and chemicalnature of herbaceous biomass with comparison of fast pyrolysisproduct distributions using Py-GC/MS. *Journal of Analytical and Applied Pyrolysis, 108,* 234–247.

Murray, H. H., & Lyons, S. C. (1959). Further correlations of kaolinite crystallinity with chemical and physical properties. *Clays and Clay Minerals, 8,* 11–17.

Odeh, A. O. (2015). Comparative study of the aromaticity of the coal structure during the cahr formation process under both conventional and advanced analytical techniques. *Energy & Fuels, 29,* 2676–2684.

Ok, Y. S., Chang, S. X., Gao, B., & Chung, H. J. (2015). SMART biochar technology—a shifting paradigm towards advanced materials and healthcare research. *Environmental Technology and Innovation, 4,* 206–209.

Qiu, M., Sun, K., Jin, J., Gao, B., Yan, Y., Han, L., et al. (2014). Properties of the plant- and manure-derived biochars and their sorption of dibutyl phthalate and phenanthrene. *Scientific Reports, 4,* 5295. doi:10.1038/srep05295.

Rajapaksha, A. U., Chen, S. S., Tsang, D. C. W., Zhang, M., Vithanage, M., Mandal, S., et al. (2016). Engineered/designer biochar for contaminant removal/immobilization from soil and water: Potential and implication of biochar modification. *Chemosphere, 148,* 276–291.

Rawal, A., Joseph, S. D., Hook, J. M., Chia, C. H., Munroe, P. R., Donne, S., et al. (2016). Mineral–Biochar composites: Molecular structure and porosity. *Environmental Science and Technology, 50,* 7706–7714.

Rumpel, C., Gonzalez-Perez, J. A., Bardoux, G., Largeau, C., Gonzalez-Vila, F. J., & Valentin, C. (2007). Composition and reactivity of morphologically distinct charred materials left after slash-and-burn practices in agricultural tropical soils. *Organic Geochemistry, 38,* 911–920.

Scheirs, J., Camino, G., & Tumiatti, W. (2001). Overview of water evolution during the thermal degradation of cellulose. *European Polymer Journal, 37,* 933–942.

Schmidt, M. W. I., & Noack, A. G. (2000). Black carbon in soils and sediments: Analysis, distribution, implications, and

current challenges. *Global Biogeochemical Cycles, 14,* 777–793.

Spokas, K. A. (2010). Review of the stability of biochar in soils: Predictability of O: C molar ratios. *Carbon Management, 1,* 289–303.

Usman, A. R. A., Abduljabbar, A., Vithanage, M., Ok, Y. S., Ahmad, M., Ahmad, M., et al. (2015). Biochar production from date palm waste: Charring temperature induced changes in composition and surface chemistry. *Journal of Analytical and Applied Pyrolysis, 115,* 392–400.

Wang, Y., Lu, H., Liu, Y., & Yang, S. (2016). Removal of phosphate from aqueous solution by SiO_2^-biochar nanocomposites prepared by pyrolysis of vermiculite treated algal biomass. *RSC Advances, 6,* 83534–83546.

Windeatt, J. H., Ross, A. B., Williams, P. T., Forster, P. M., Nahil, M. A., & Singh, S. (2014). Characteristics of biochars from crop residues: Potential for carbon sequestration and soil amendment. *Journal of Environmental Management, 146,* 189–197.

Xiao, X., Chen, B., & Zhu, L. (2014). Transformation, morphology and dissolution of silicon and carbon in rice straw derived biochars under different pyrolytic temperatures. *Environmental Science and Technology, 48,* 3411–3419.

Yang, H., Yan, R., Chen, H., Lee, D. H., & Zheng, C. (2007). Characteristics of hemicellulose, cellulose and lignin pyrolysis. *Fuel, 86,* 1781–1788.

Yao, Y., Gao, B., Fang, J., Zhang, M., Chen, H., Zhou, Y., et al. (2014). Characterization and environmental applications of clay–biochar composites. *Chemical Engineering Journal, 242,* 136–143.

Zhao, L., Cao, X., Masek, O., & Zimmerman, A. (2013). Heterogeneity of biochar properties as a function of feedstock sources and production temperatures. *Journal of Hazardous Materials, 256–257,* 1–9.

Zimmerman, A. R., Gao, B., & Ahn, M. Y. (2011). Positive, negative carbon mineralization priming effects among a variety of biochar-amended soils. *Soil Biology & Biochemistry, 43,* 1169–1179.

Zimmermann, M., Bird, M. I., Wurster, C., Saiz, G., Goodrick, I., Barta, J., et al. (2012). Rapid degradation of pyrogenic carbon. *Global Change Biology, 18,* 3306–3316.